Longitudinal Emittance

Old and New Results

David H. Dowell
SLAC

Outline of Talk

The Old (1993-1997):

- **Measurements below the SC Limit at ELSA**

The New (2000-Present):

- **Measurements performed at SLAC Gun Test Facility**
- **Linear, rms analysis**
- **Tomographic Reconstructions of Phase Space Distributions (H. Loos, BNL)**
- **Tomography of DUV-FEL Beam (H. Loos, BNL)**

The 'Old', Circa. 1993

CEA, Bruyeres-le-Chatel, France:
S. Joly
A. Loulergue
G. Haouat
J.P. de Brion

Components of the ELSA Accelerator Used to Make the Longitudinal Phase Space Measurements

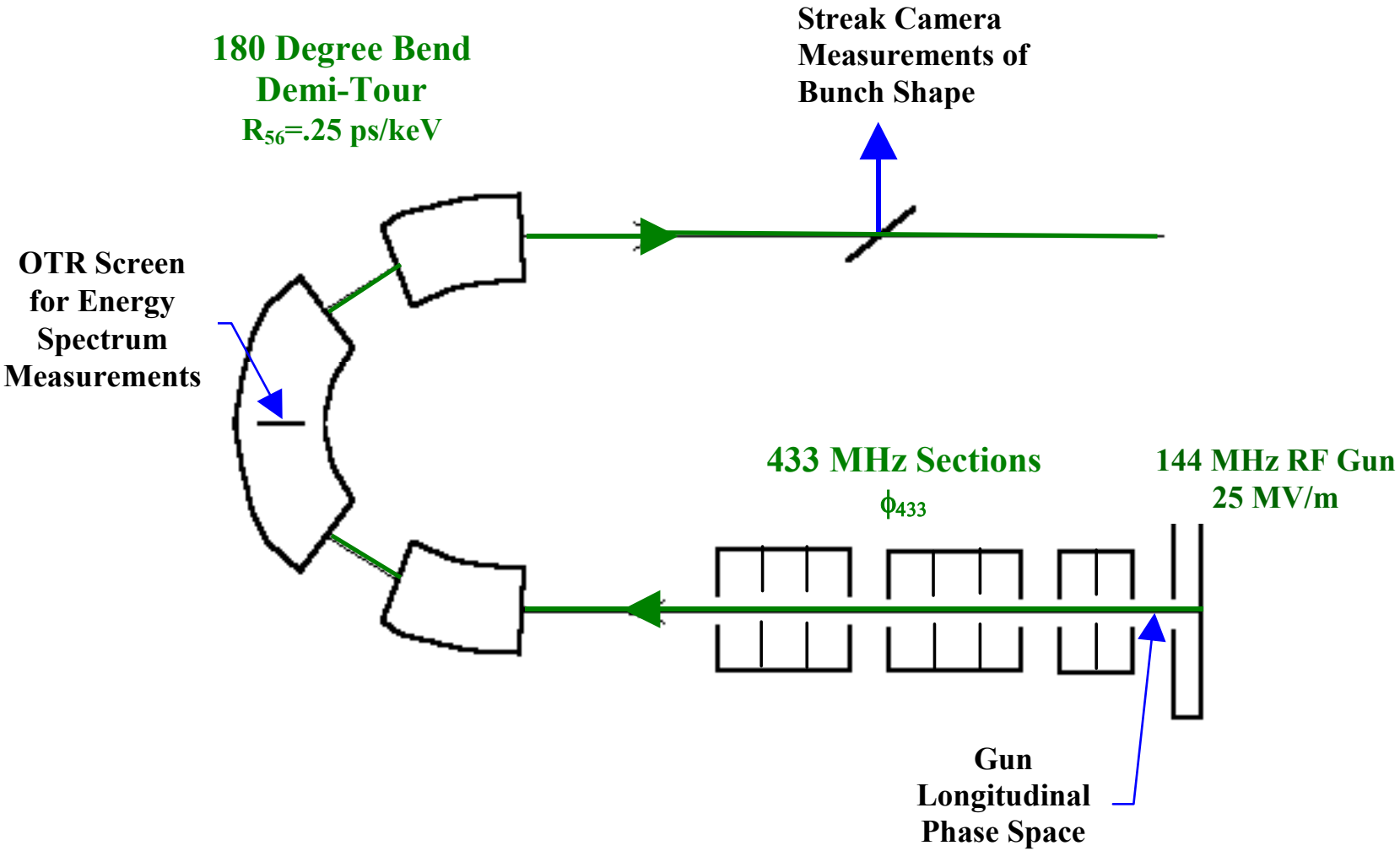

Definition of Phase Space Parameters, Including Correlations

Longitudinal Beam Ellipse:

$$\gamma\Delta t^2 + 2\alpha\Delta t\Delta E + \beta\Delta E^2 = \frac{\varepsilon_\ell}{\pi}$$

Longitudinal Beam Matrix:

$$\tau = \begin{pmatrix} \tau_{11} & \tau_{12} \\ \tau_{12} & \tau_{22} \end{pmatrix} = \varepsilon_\ell \begin{pmatrix} \beta & \alpha \\ \alpha & \gamma \end{pmatrix}$$

$\sqrt{\tau_{11}}$ = Uncorrelated Bunch Length

$\sqrt{\tau_{22}}$ = Uncorrelated Energy Spread

Include correlated emittance by distorting the ellipse boundary using quadratic and cubic terms:

$$\Delta E = -\frac{\alpha}{\beta}\Delta t \pm \sqrt{\left(\frac{\alpha}{\beta}\Delta t\right)^2 - \frac{\gamma\Delta t^2 - \frac{\varepsilon_\ell}{\pi}}{\beta}} + a\Delta t^2 + b\Delta t^3$$

Randomly populate and ray-trace down the 433 MHz accelerator:

$$\Delta E_1 = \Delta E_0 + E_{433}(\cos(\phi_{433} + \Delta t_0) - \cos(\phi_{433})) \quad ; \quad \Delta t_1 = \Delta t_0$$

And continue ray-tracing around the Demi-Tour:

$$\Delta E_2 = \Delta E_1 \quad ; \quad \Delta t_2 = \Delta t_1 + R_{56}\Delta E_1$$

Distortions of the Longitudinal Phase Space Ellipse

Undistorted Phase Space
$\tau_{12} = 0$
$a = 0,\ b = 0$

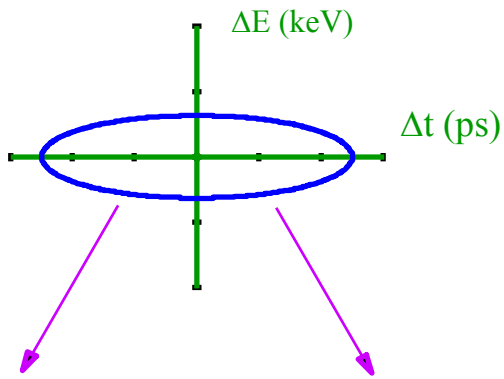

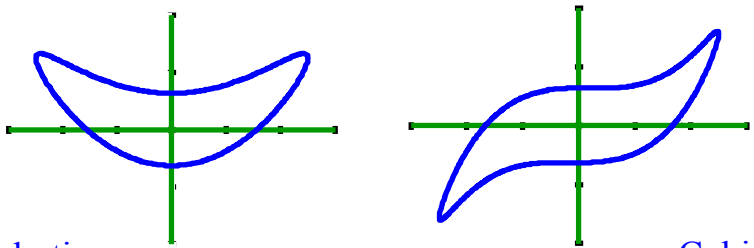

Quadratic
Distortion
$\tau_{12} = 0$
$a > 0,\ b = 0$

Cubic
Distortion
$\tau_{12} = 0$
$a = 0,\ b > 0$

Fits to 1 nC per Microbunch Data

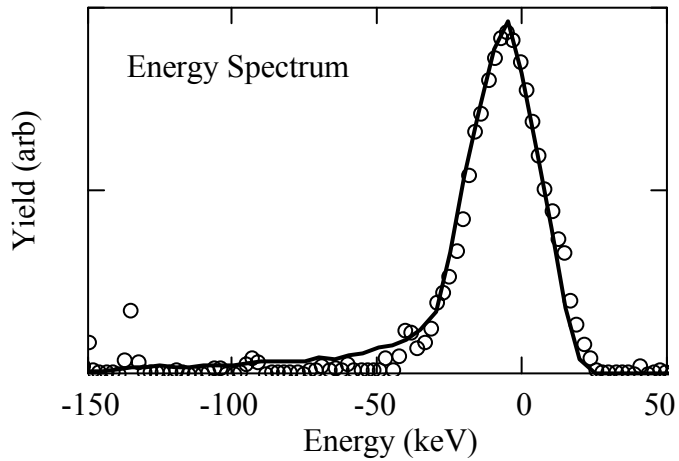

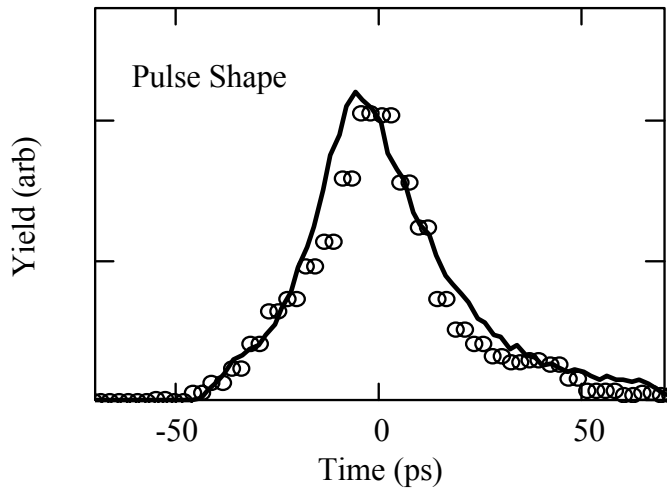

Longitudinal Phase Space Distributions Obtained from the Data Analysis

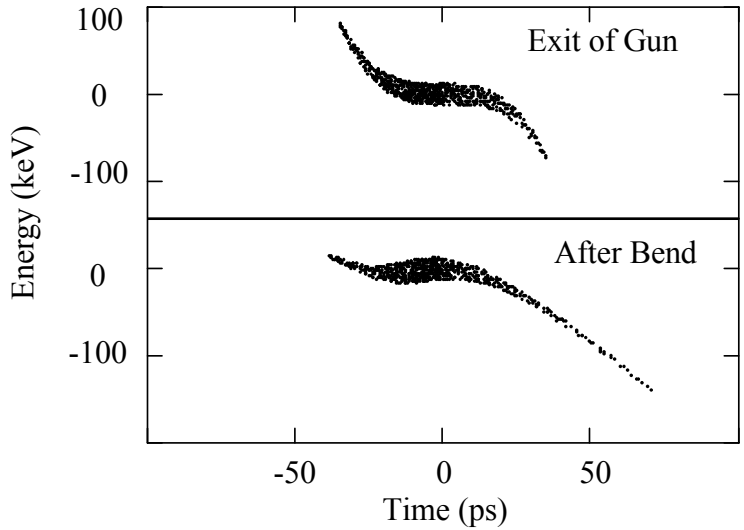

Ref: S. Joly et al.,...

Longitudinal Phase Spaces at Entrance to Main Accelerator Section

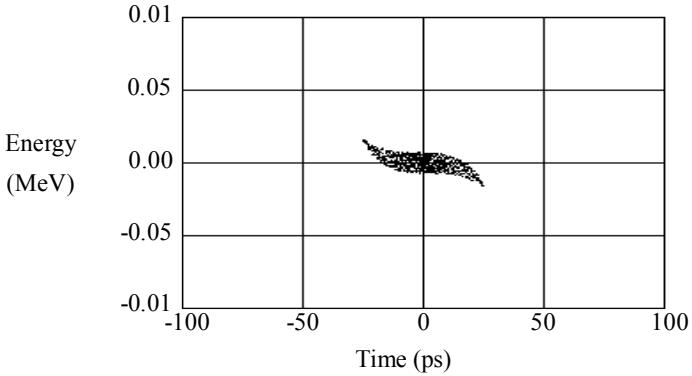

0.5 nC per micropulse

133 A/cm^2 Peak Current Density

$\tau_{11} = 25^2$ ps^2

$\tau_{12} = 0$

$\tau_{22} = 7^2$ KeV^2

$a = 0, b = -1 \times 10^{-6}$ MeV/ps^3

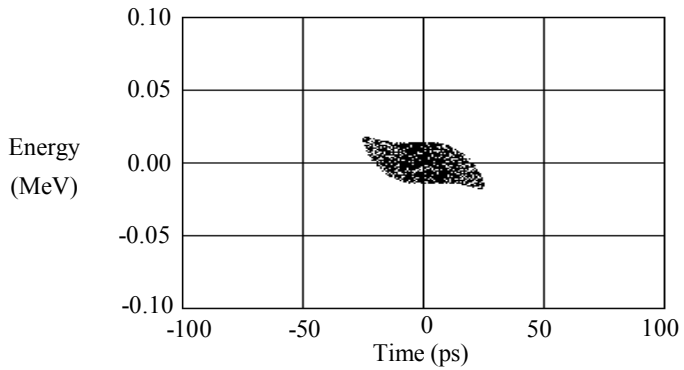

1.0 nC per micropulse

265 A/cm^2 Peak Current Density

$\tau_{11} = 25^2$ ps^2

$\tau_{12} = 0$

$\tau_{22} = 14^2$ KeV^2

$a = 0, b = -1 \times 10^{-6}$ MeV/ps^3

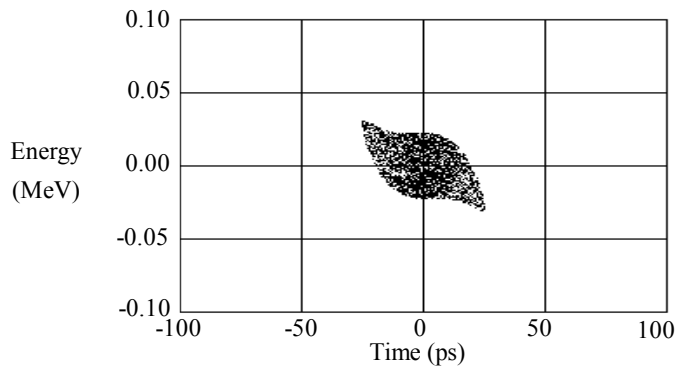

2.0 nC per micropulse

530 A/cm^2 Peak Current Density

$\tau_{11} = 25^2$ ps^2

$\tau_{12} = 0$

$\tau_{22} = 22^2$ KeV^2

$a = 0, b = -1.8 \times 10^{-6}$ MeV/ps^3

The Uncorrelated Emittance Grows Linearly with Surface Charge Densities Below the Space Charge Limit

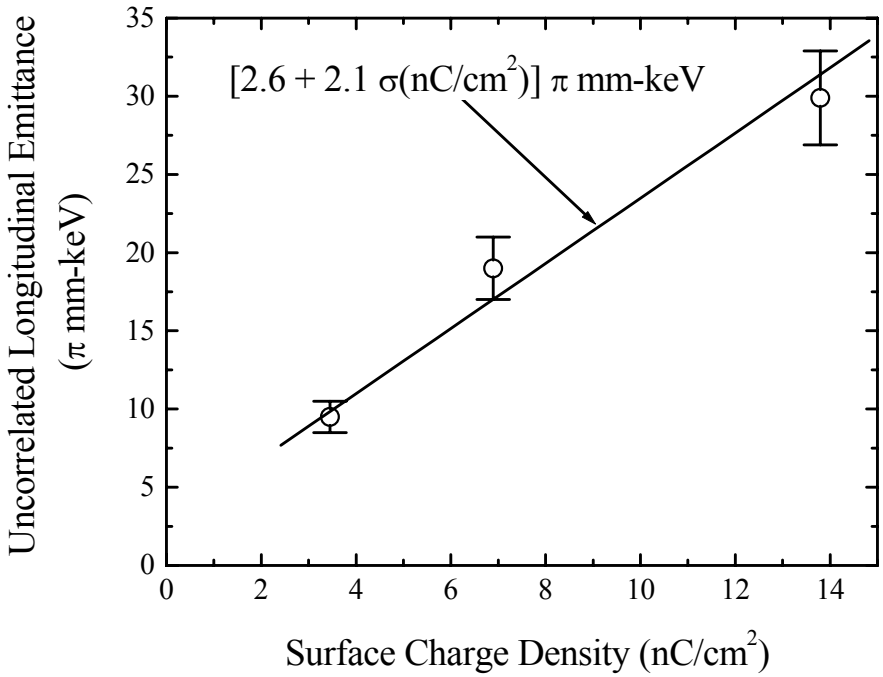

In These Experiments Most of the Emittance Growth Was due to Increased Energy Spread

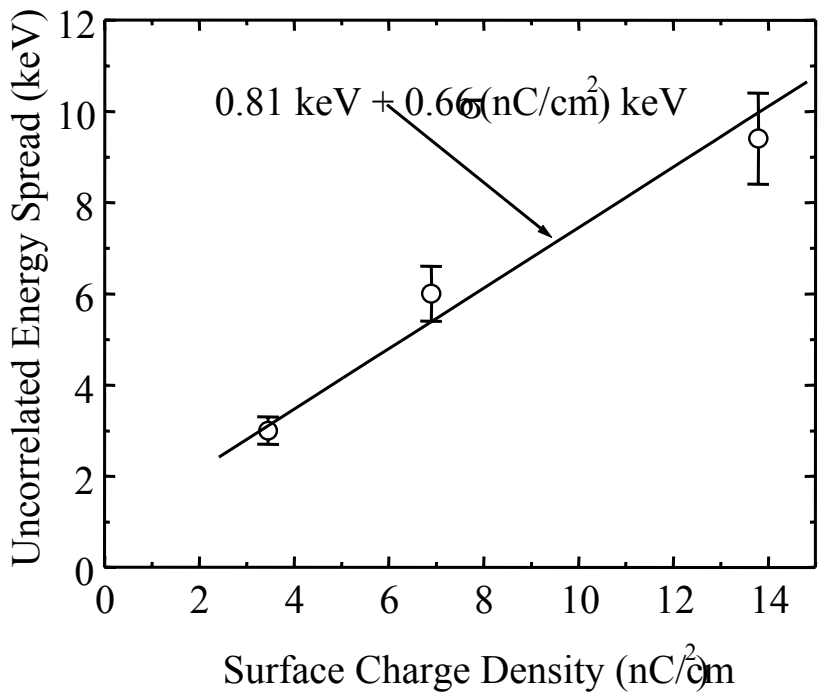

Pulse length a constant 11 ps(rms)

10 nC/cm² corresponds to 11 MV/m

Ref: D.H. Dowell et al., PAC97.

The 'New', Circa. 2003

SLAC Gun Test Facility

P.R. Bolton
J.E. Clendenin
D.H. Dowell
S.M. Gierman
C.G. Limborg
B.F. Murphy
J.F. Schmerge

BNL DUV-FEL

A. Doyuran
W. Graves
J. Greco
H. Loos
J.B. Murphy
J. Rose
T.V. Shaftan
B. Sheehy
Y. Shen
B. Singh
X.J. Wang
Z. Wu
L.H. Yu

GTF Diagnostics and Transport

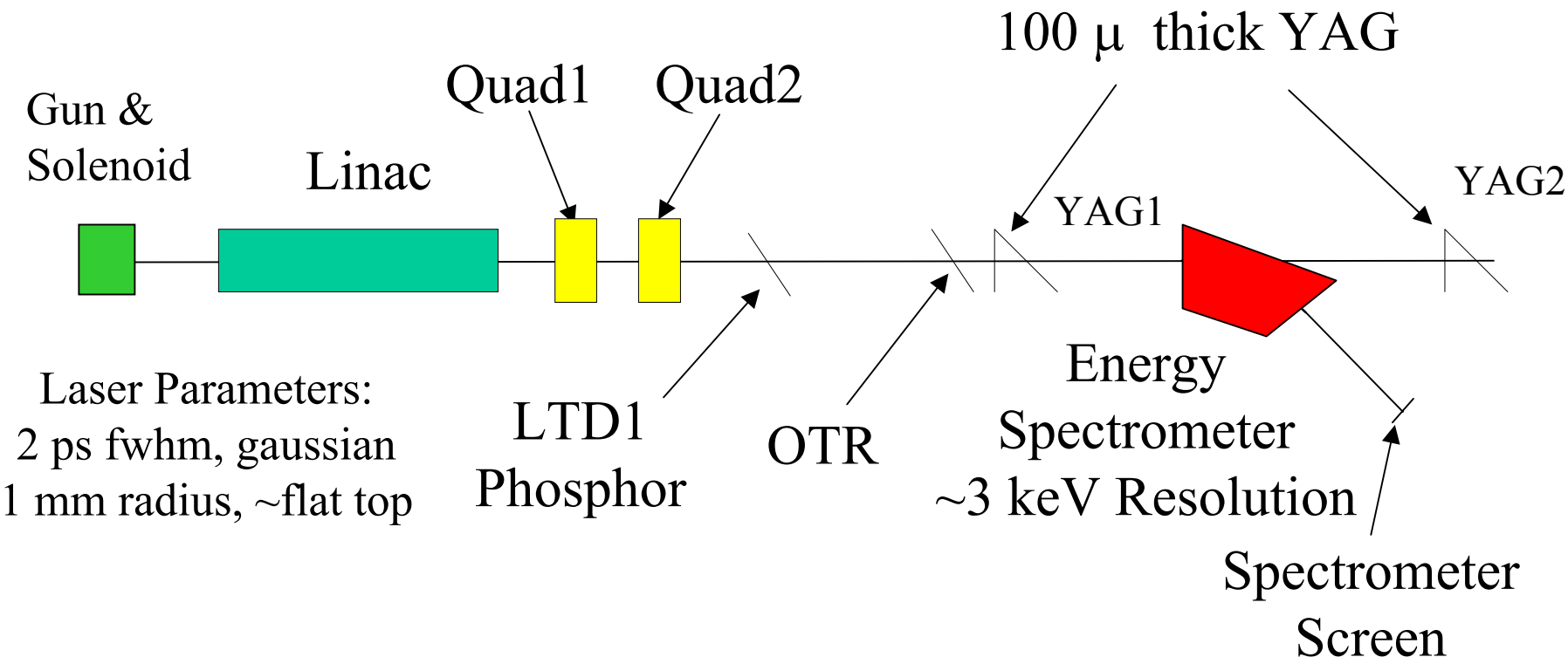

Linear Longitudinal Analysis

Symmetric longitudinal beam matrix:

$$\tau = \begin{pmatrix} \tau_{11} & \tau_{12} \\ \tau_{12} & \tau_{22} \end{pmatrix} \quad ; \quad \tau_{11} = \sigma_{t,\phi}^2 \quad ; \quad \tau_{22} = \sigma_E^2$$

$$\tau(\text{spectrometer}) = R_{acc}\,\tau(\text{gun} + \text{drift})R_{acc}^{T}$$

$$R_{acc} = \begin{pmatrix} 1 & 0 \\ -V_{acc}\sin\phi & 1 \end{pmatrix}$$

$$\tau(\text{spectrometer}) = \begin{pmatrix} \tau_{11} & \tau_{12} - \tau_{11}V_{acc}\sin\phi \\ \tau_{12} - \tau_{11}V_{acc}\sin\phi & \tau_{22} - V_{acc}\sin\phi(2\tau_{12} - \tau_{11}V_{acc}\sin\phi) \end{pmatrix}$$

$$\sigma_E{}^2(\text{spectrometer}) = \tau_{22} - V_{acc}\sin\phi(2\tau_{12} - \tau_{11}V_{acc}\sin\phi)$$

Find τ_{11}, τ_{12}, τ_{22} by fitting energy spread vs. linac phase

Experimental Energy Spread at Low and Moderate Charge Phase-Scan Measurements

15 pC Data with Fit

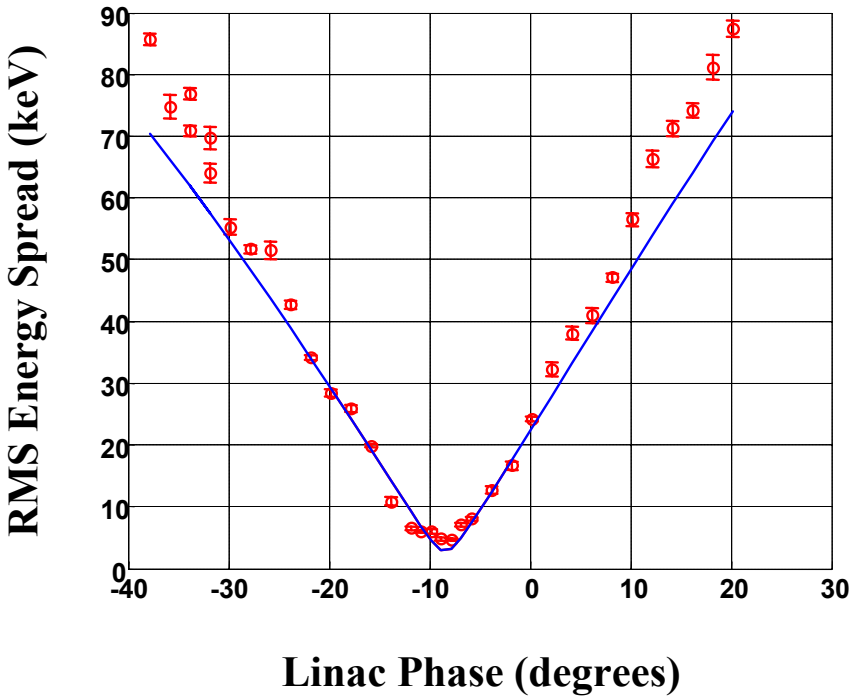

300 pC Data with Fit

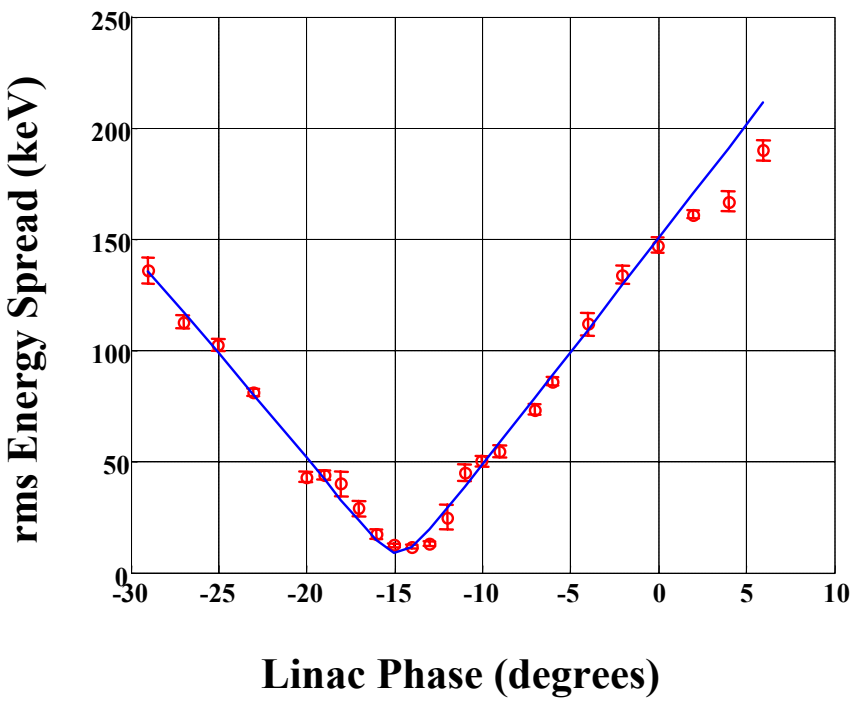

Comparison of Longitudinal Phase Spaces

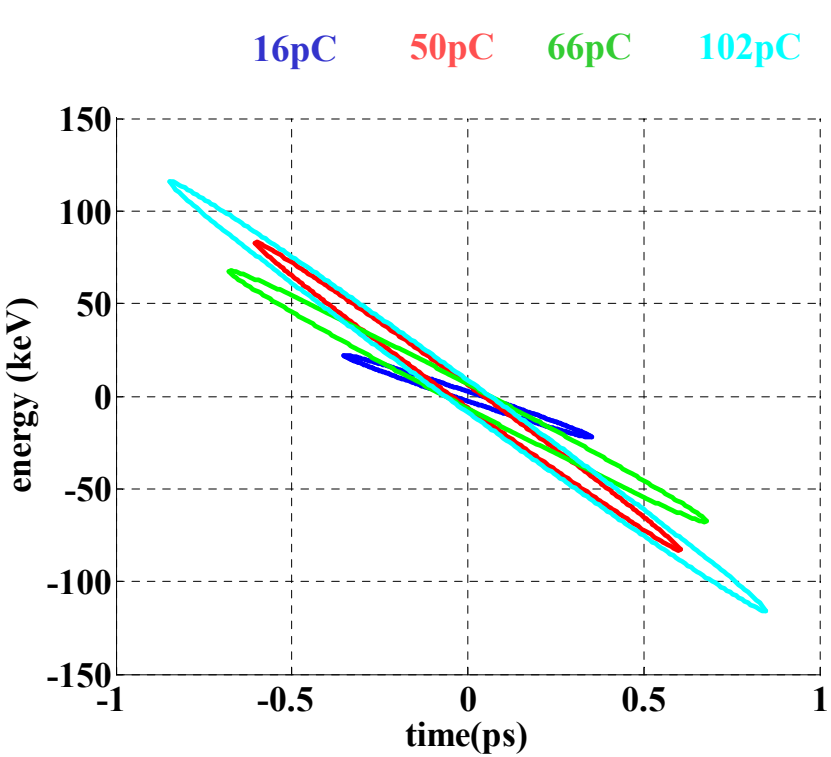

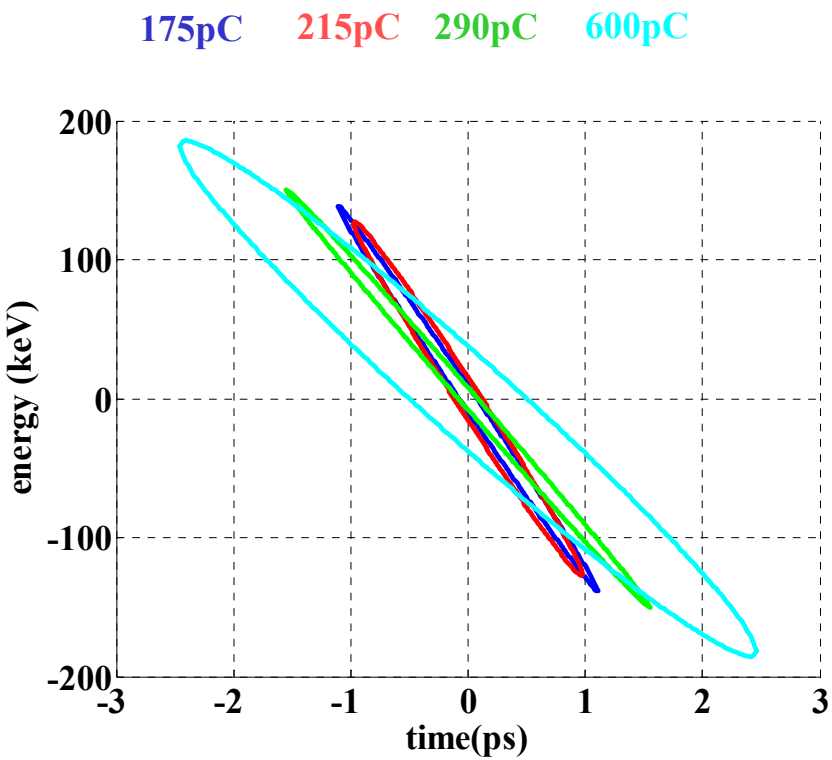

Results of the Linear Longitudinal Analysis

Initial Conditions:
Drive Laser Pulse Width
~2ps(fwhm), 0.85ps (rms), gaussian
Spot size = 1mm radius (~uniform)
Launch Phase = 30 degrees
Peak Field = 110 MV/m

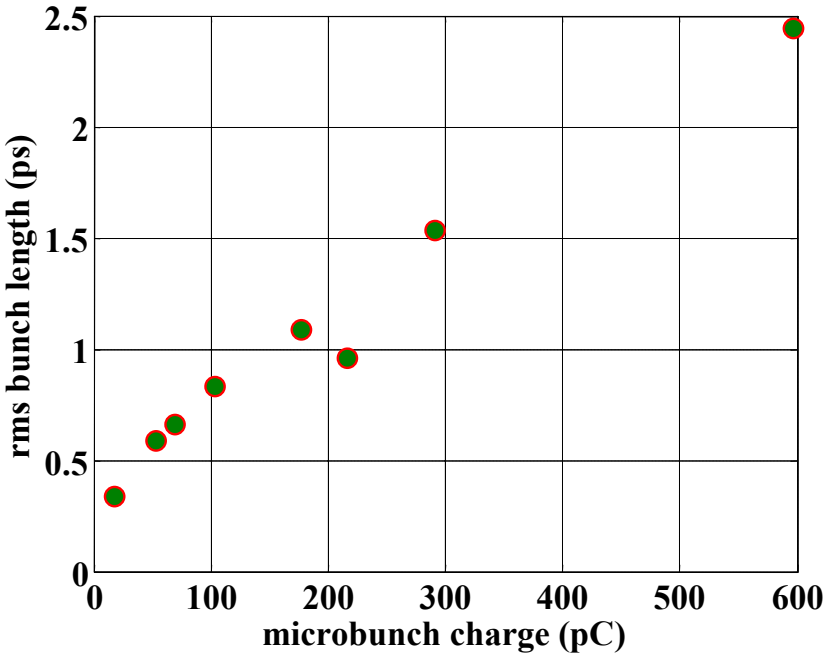

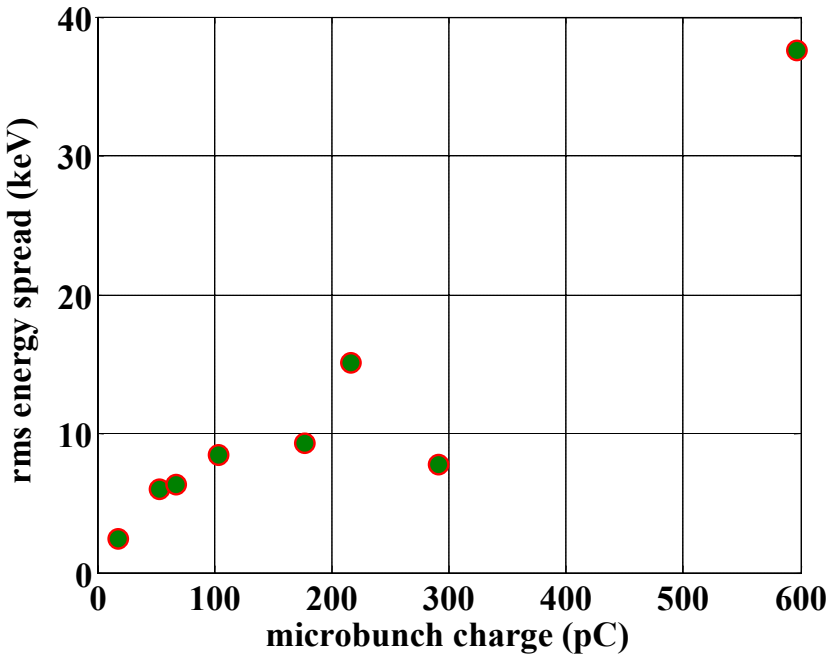

Longitudinal Phase Space Tomography at SLAC GTF and BNL DUV-FEL

H. Loos*, P.R. Bolton†, J.E. Clendenin†, D.H. Dowell†, S.M. Gierman†, C.G. Limborg†, J.F. Schmerge†, T.V. Shaftan*, B. Sheehy*

*National Synchrotron Light Source, BNL
†Stanford Linear Accelerator Center

Presented at 25th Free Electron Laser Conference

Slide compliments of H. Loos, BNL

Outline

- Motivation & facilities
- Tomographic reconstruction
  - Algebraic reconstruction technique (ART)
  - Other methods (Fourier, maximum entropy)
- GTF results
  - 15 pC example
  - Studied systematics from low to high charge
- DUV-FEL results
- Summary and outlook

Slide compliments of H. Loos, BNL

Motivation

Longitudinal phase space tomography is useful for:

- Model independent determination of the phase space distribution.
- Measurement of local energy spread.
- Provides experimental basis for bunch compression analysis.
- Benchmarking of simulation codes.

Slide compliments of H. Loos, BNL

ART and Other Methods

- Filtered Backprojection
  - Developed for rotation of geometric object.
  - No unique definition of angle in phase space.
  - Inter- and extrapolation of projections necessary.
- ART
  - Works for arbitrary set of linear and nonlinear phase space transformations.
  - Constraints on solution can be implemented.
- MENT (Maximum Entropy)
  - Guarantees nonnegative solution.
  - Better suppression of artifacts than ART
  - Not yet implemented here…

Slide compliments of H. Loos, BNL

Algebraic Reconstruction Technique

- Many different transformations of an image g generate a set of histograms or projections p_i.
- Find the transport matrix a_i, so that $p_{i,j} = \Sigma_{jl}\, a_{i,jl}\, g_l$.
- The algorithm iterates an initial guess $g^{(0)}$ for each projection i according to

$$g_q^{(k+1)} = g_q^{(k)} + \Sigma_j \left[a_{i,jq} \left(p_{i,j} - \Sigma_l\, a_{i,jl}\, g_l^{(k)} \right) / \Sigma_{nl}\, a_{i,nl}^2 \right]$$

until each projection has been used.

- Repeat until convergence achieved.

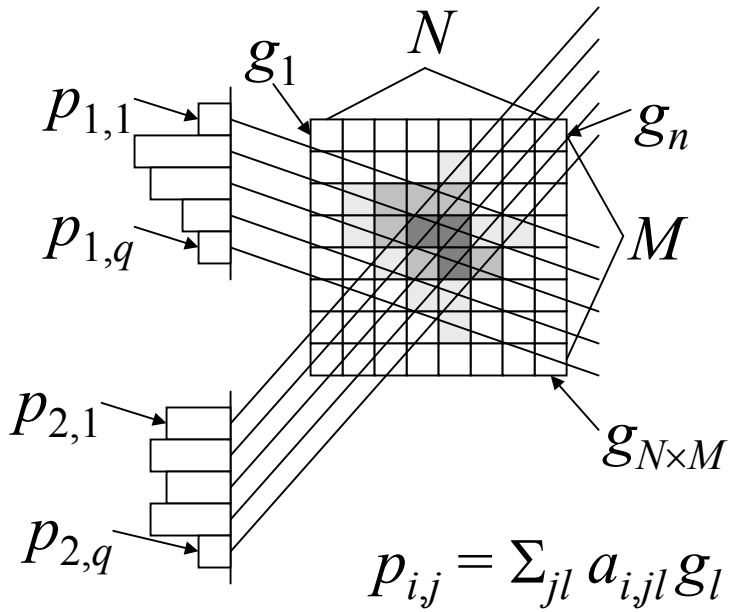

Slide compliments of H. Loos, BNL

Analysis of GTF Longitudinal Data

Energy after linac

$E = E_0 + V \cos(\phi)$

Chirp from linac

$k = -V \omega \sin(\phi)$

Energy spread

$\sigma_\delta'^2 = \sigma_\delta^2 + 2k\sigma_{\delta\tau} + k^2\sigma_\tau^2$

- Measure acceleration gradient
- Check validity of measured profiles
- Determine initial chirp after gun

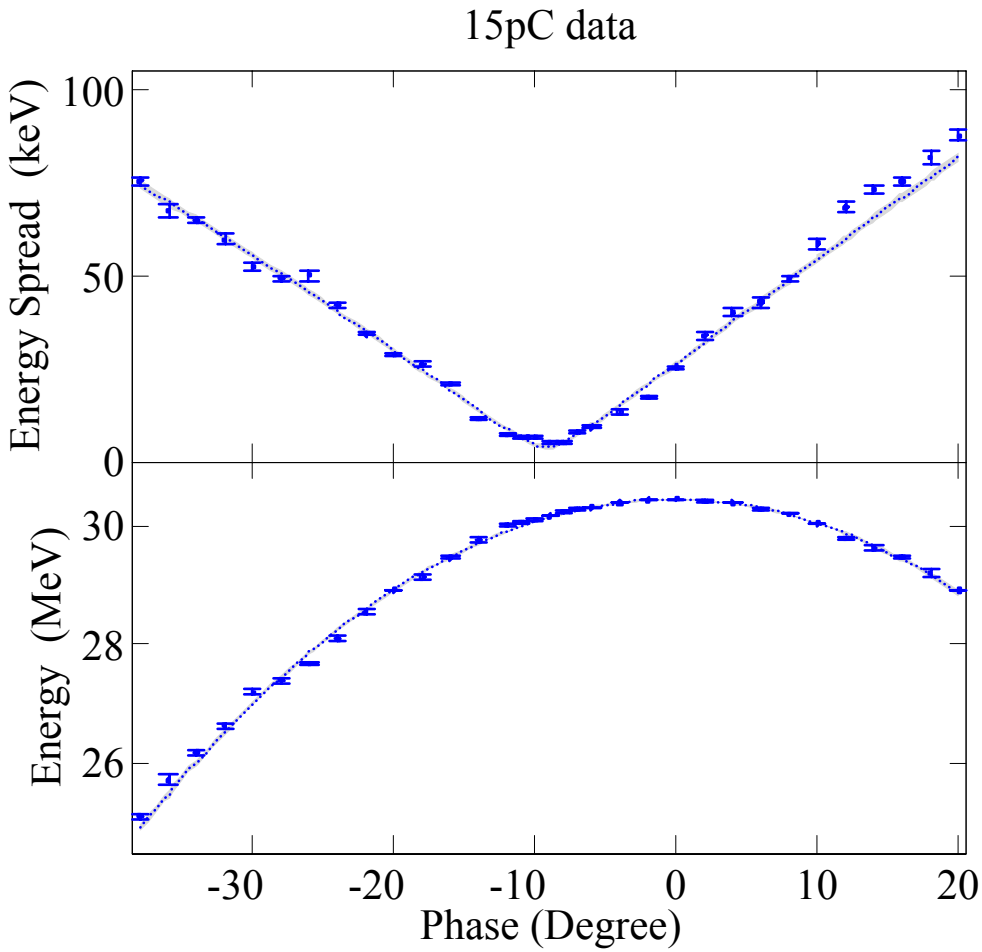

Slide compliments of H. Loos, BNL

Reconstruction for 15 pC

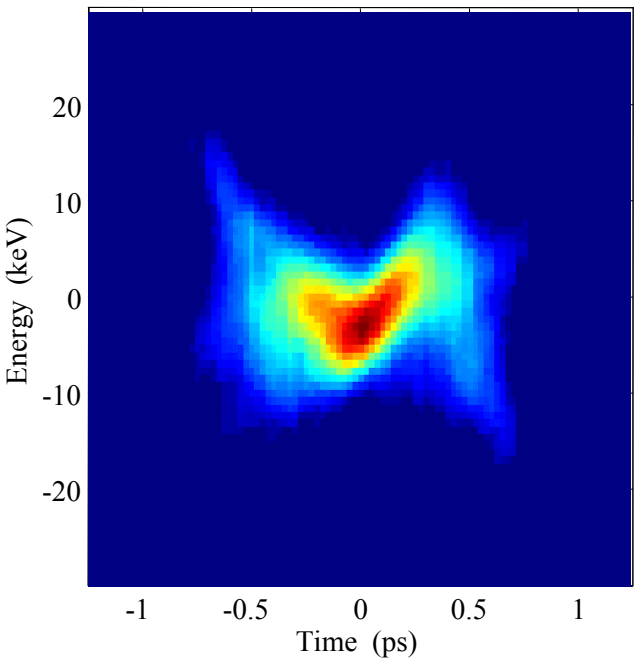

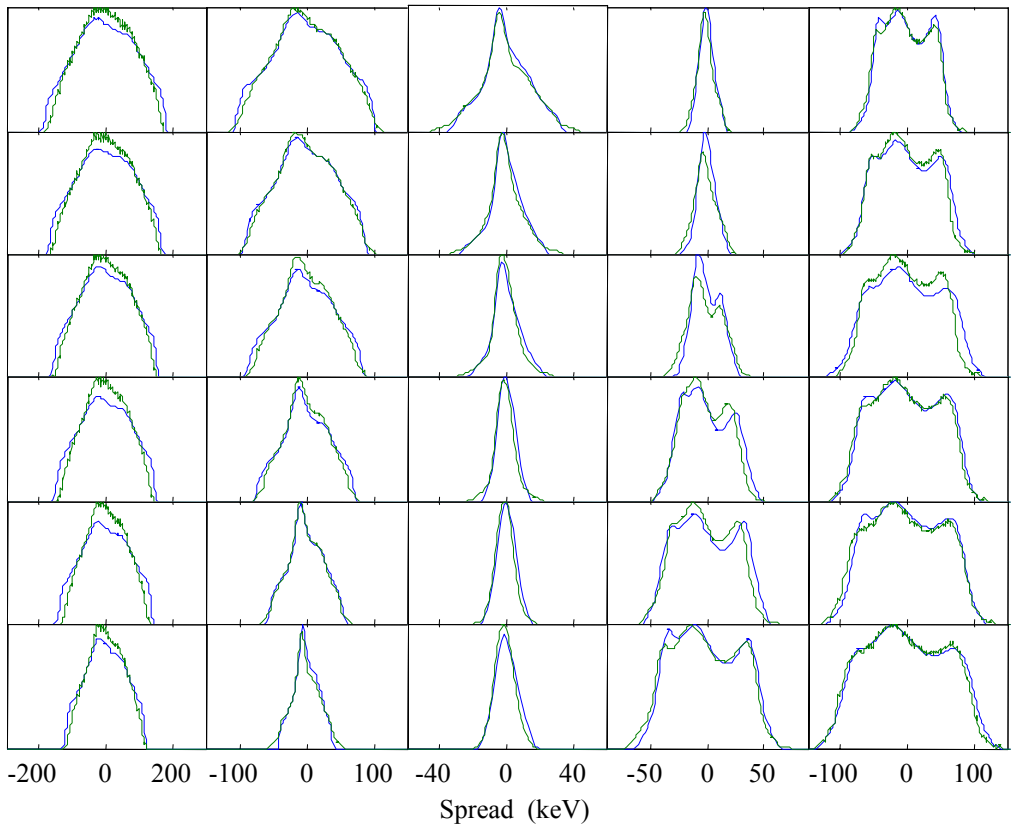

Reconstruct phase space w/o initial chirp to minimize rectangular phase space area.

Slide compliments of H. Loos, BNL

Reconstructed Phase Spaces

- Artifacts due to linac phase and amplitude drifts.
- Removal of 'streak' artifacts with 7% floor cut.
- Slice energy spread grows with charge
- Energy spread higher in bunch tail for higher charges.

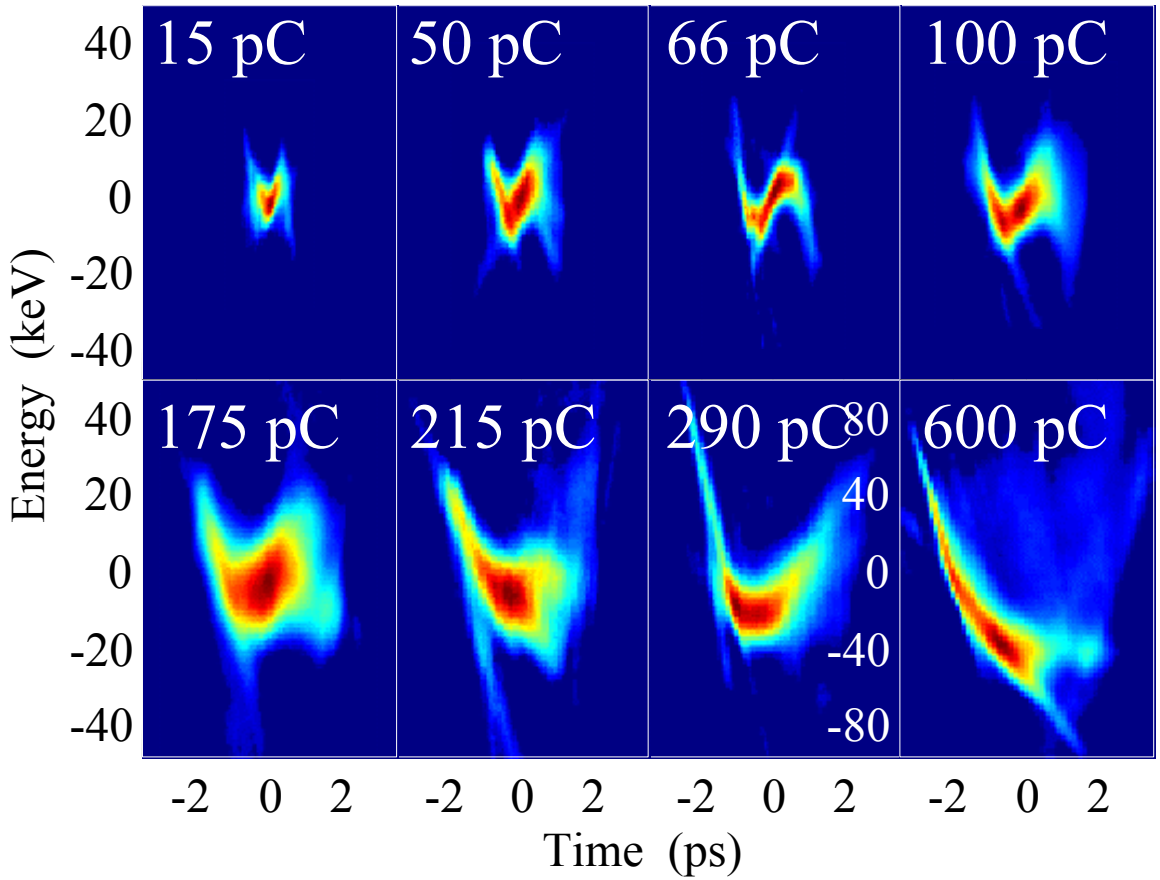

Slide compliments of H. Loos, BNL

Temporal Projections

- Compression below 100 pC and elongation above.
- Smooth time distributions showing little structure.
- Structure can be attributed to artifacts.

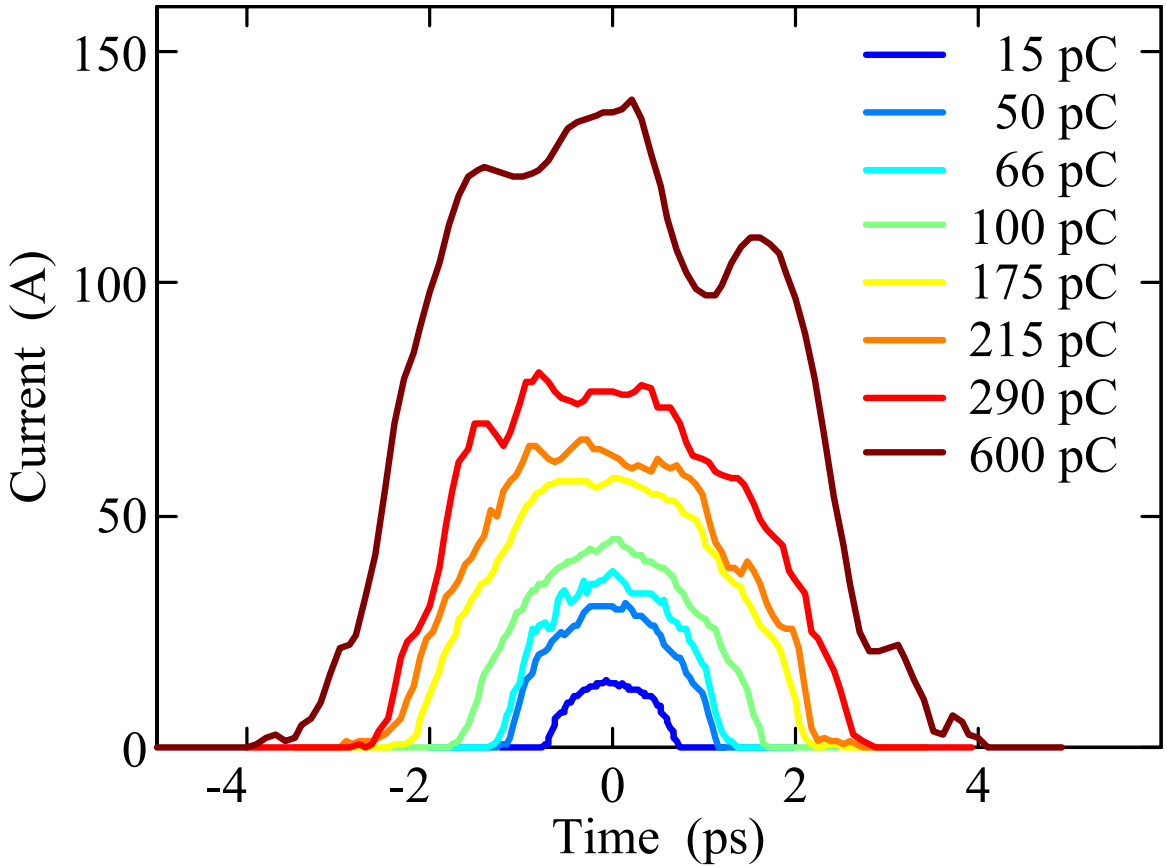

Slide compliments of H. Loos, BNL

Energy Spread Analysis

- Slice energy spread determined by gaussian fit to each slice.

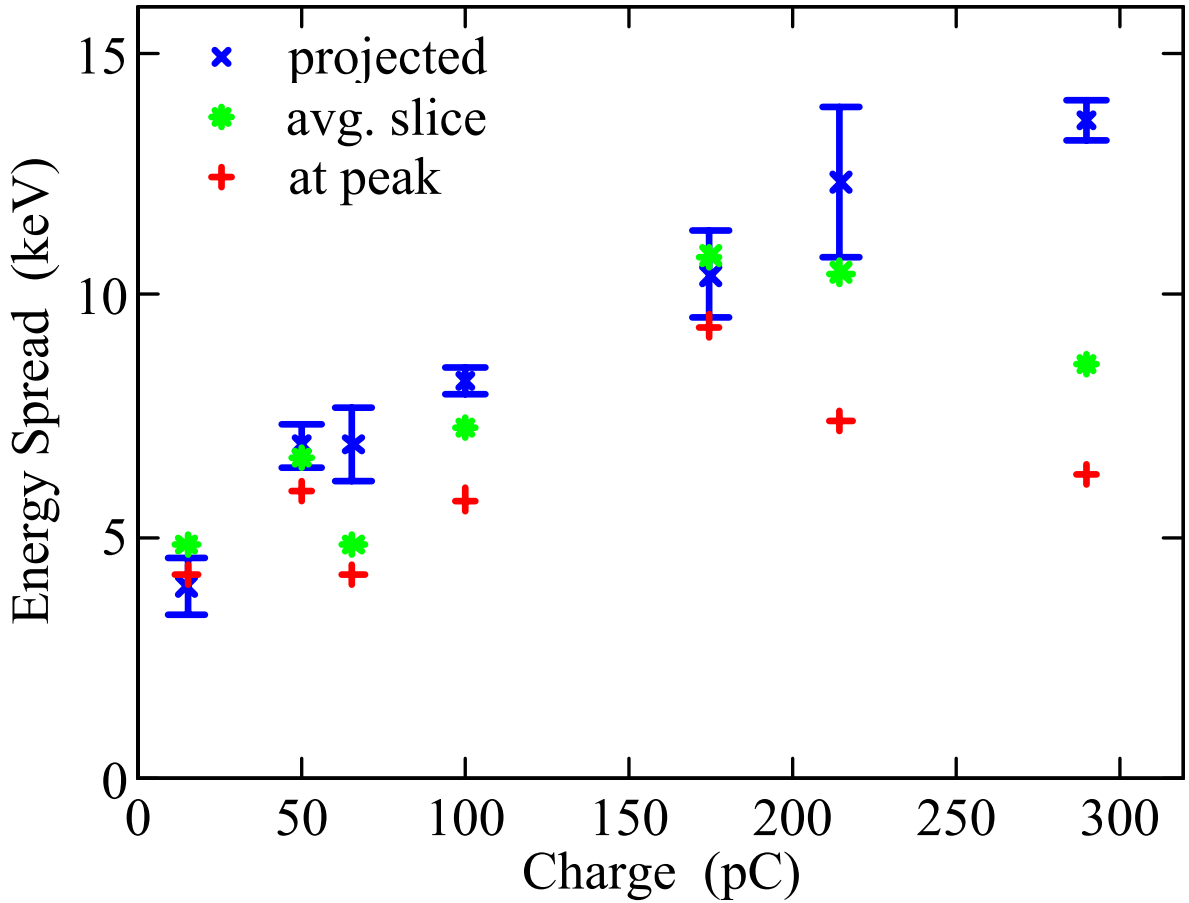

Slide compliments of H. Loos, BNL

Longitudinal Emittance

Normalized emittance

$\varepsilon_n = \varepsilon[\mathrm{keV}]/m_0c$

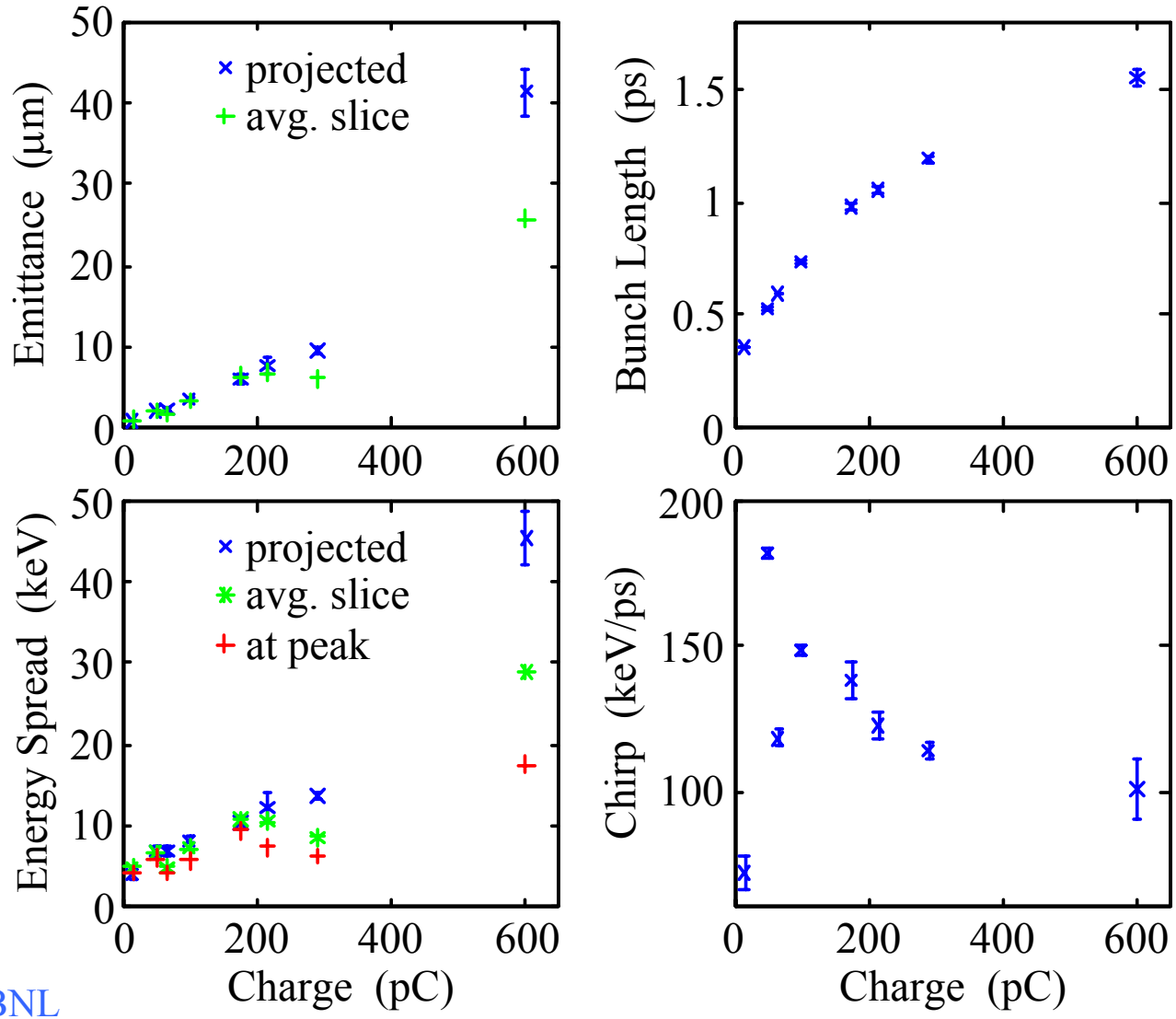

Slide compliments of H. Loos, BNL

dowell@slac.stanford.edu

DUV-FEL Phase Space

200 pC charge, 38 MeV gain in Tank1
200 keV/ps max. chirp, f_{Res} = 4 THz

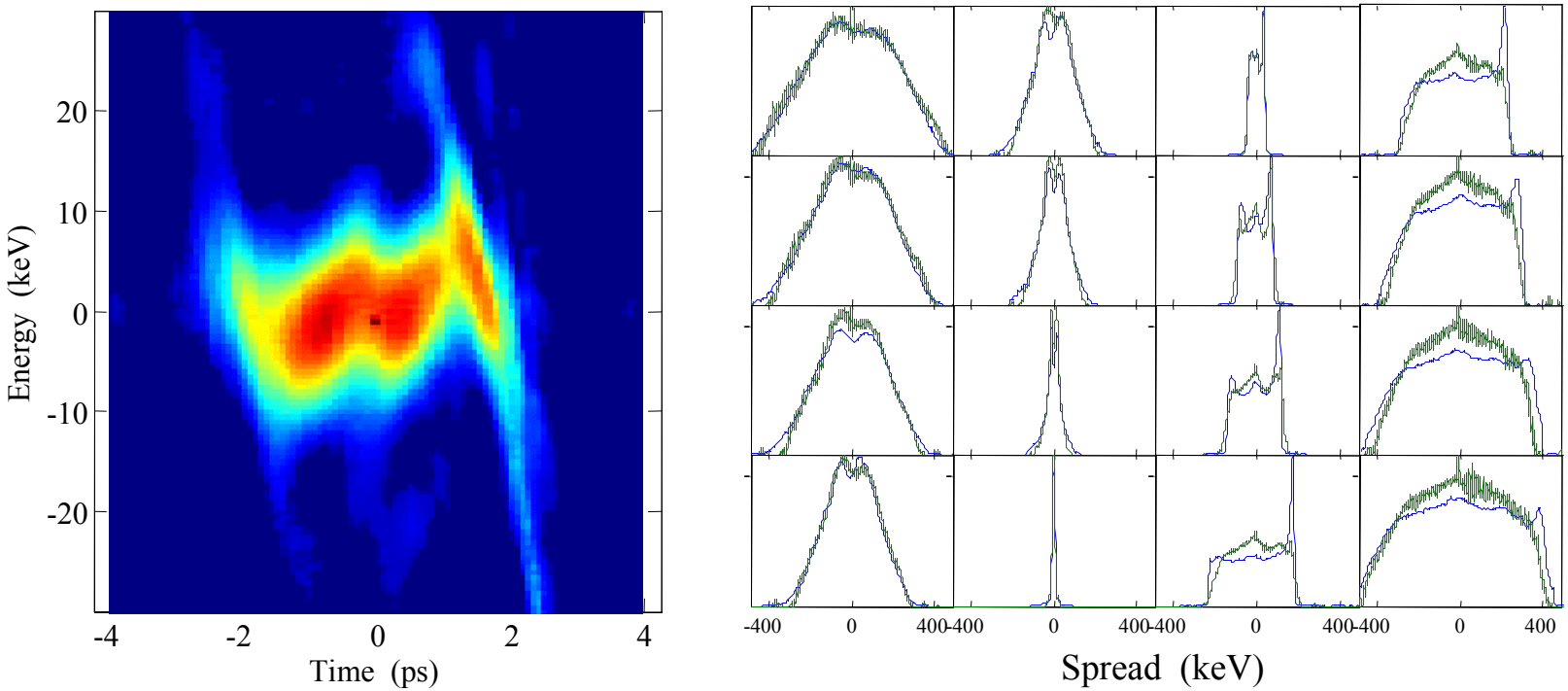

Slide compliments of H. Loos, BNL

Comparison with Laser Profile

- e-beam 1.35 ps
- laser 2.35 ps
- 8 keV slice energy spread
- Structure of laser not apparent in electron beam distribution.
- Structure visible only in energy correlation.

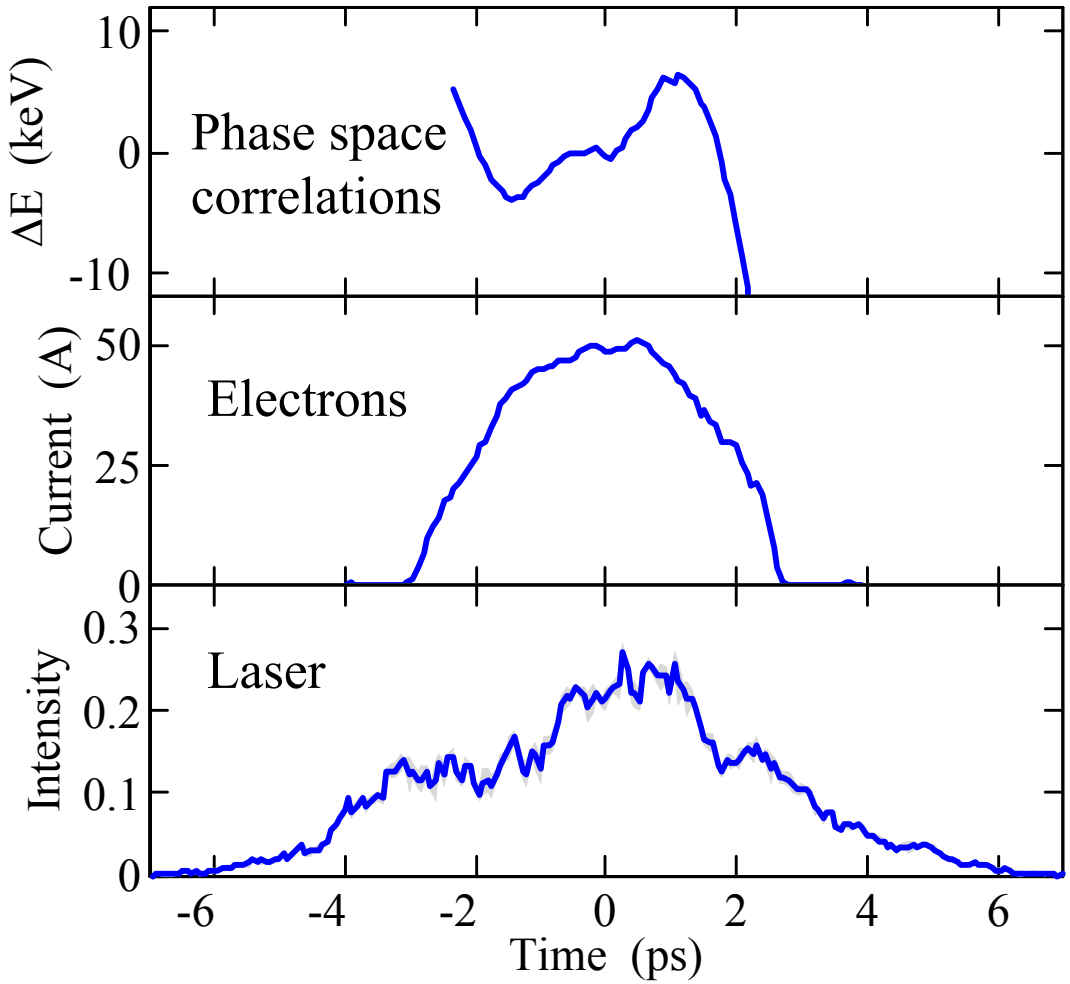

Slide compliments of H. Loos, BNL

Summary and Outlook

- GTF accelerator provides reproducible electron beam required for tomography.
- Phase space reconstructions for charges from 15 to 600 pC obtained.
- Slice energy spread between 0% and 60% smaller than projected energy spread.
- Comparison with simulation in progress.
- Phase space reconstruction of compressed beam at DUV-FEL planned, needs highly reproducible beam!

Slide compliments of H. Loos, BNL

Virtual Cathode Effects

D.H. Dowell
SLAC

The 'Old', Circa. 1993

CEA, Bruyeres-le-Chatel, France:
S. Joly
A. Loulergue
G. Haouat
J.P. de Brion

D.H. Dowell, S. Joly, A. Loulergue, J.P. deBrion and G. Haouat, Phys. Plasmas 4, 3369(1997)

Components of the ELSA Accelerator Used to Make the Longitudinal Phase Space Measurements

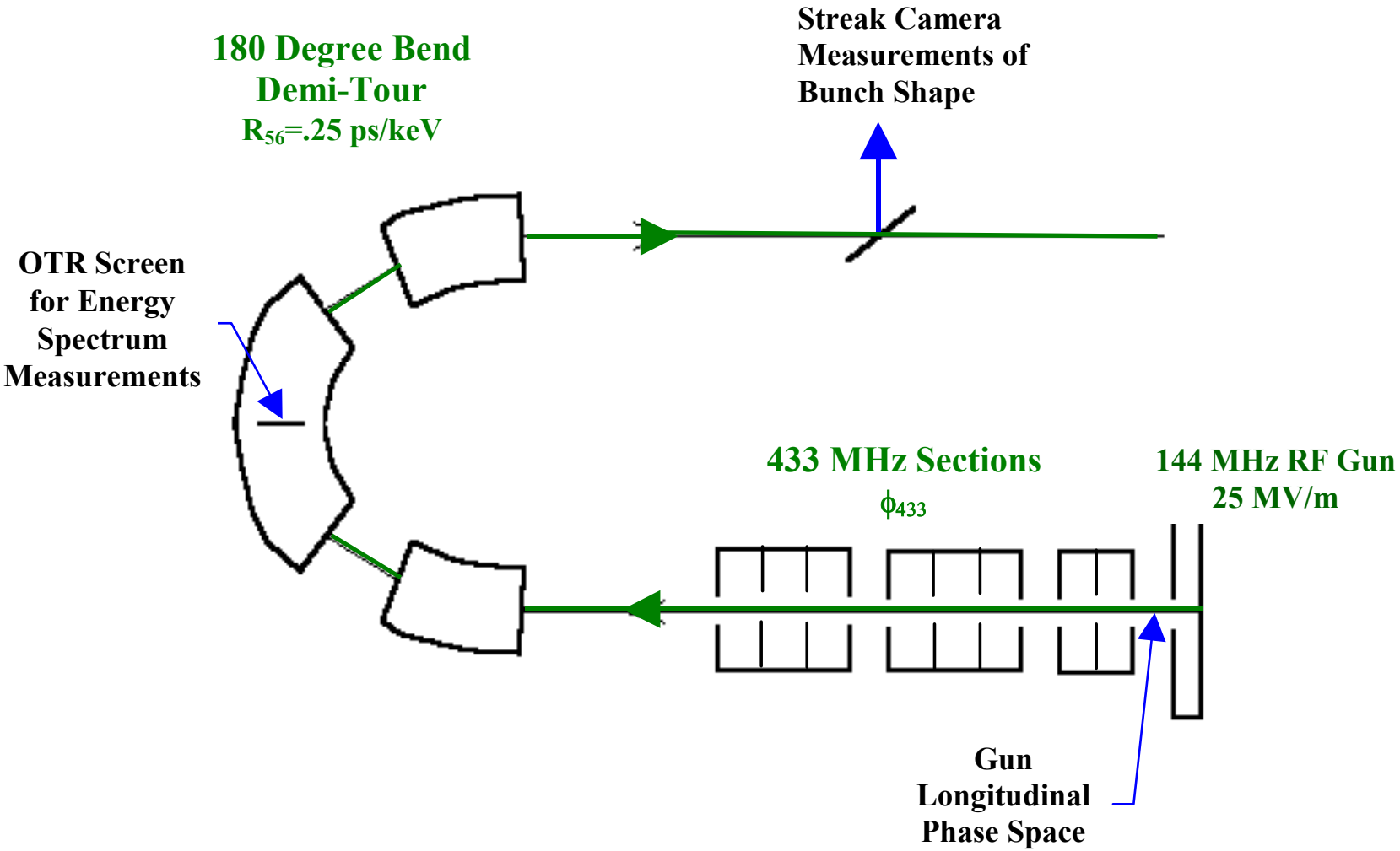

Streak Camera Measurements Showing Onset of Virtual Cathode

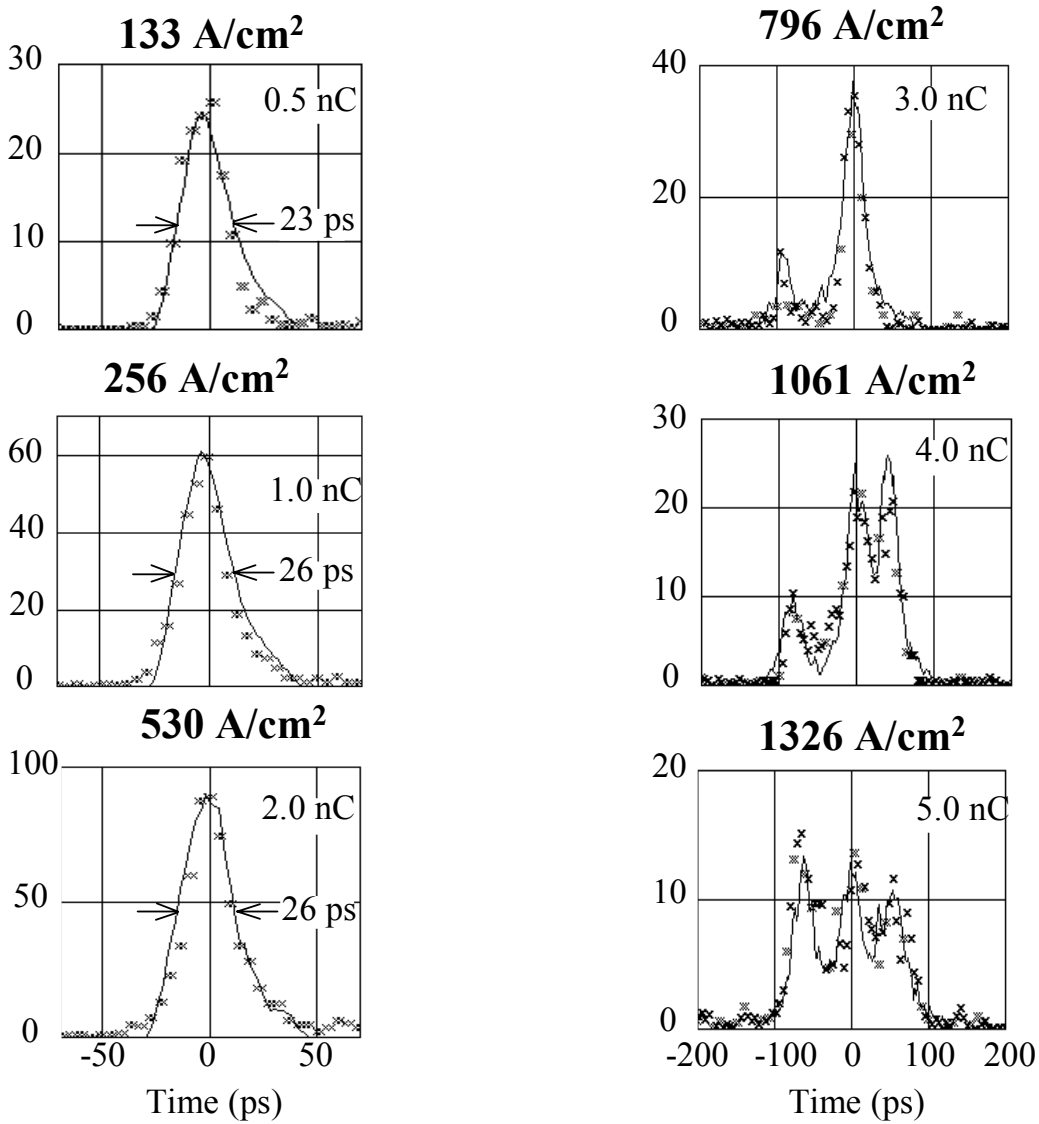

Cathode Peak Field 21 MV/m
Launch Phase ~ 60 degrees
Space Charge Limit:
Child's Law ~250 A/cm²

$$J_{Childs} = 2.33\times10^{-2}\frac{V_0^{3/2}}{d^2} \quad [A/cm^2]$$

V_0 is the voltage across gap d

See Reiser, "Theory and Design of Particle Beams"

Fits to Parameterized Phase Space Distributions

Space Charge Limit: Child's Law ~250 A/cm^2

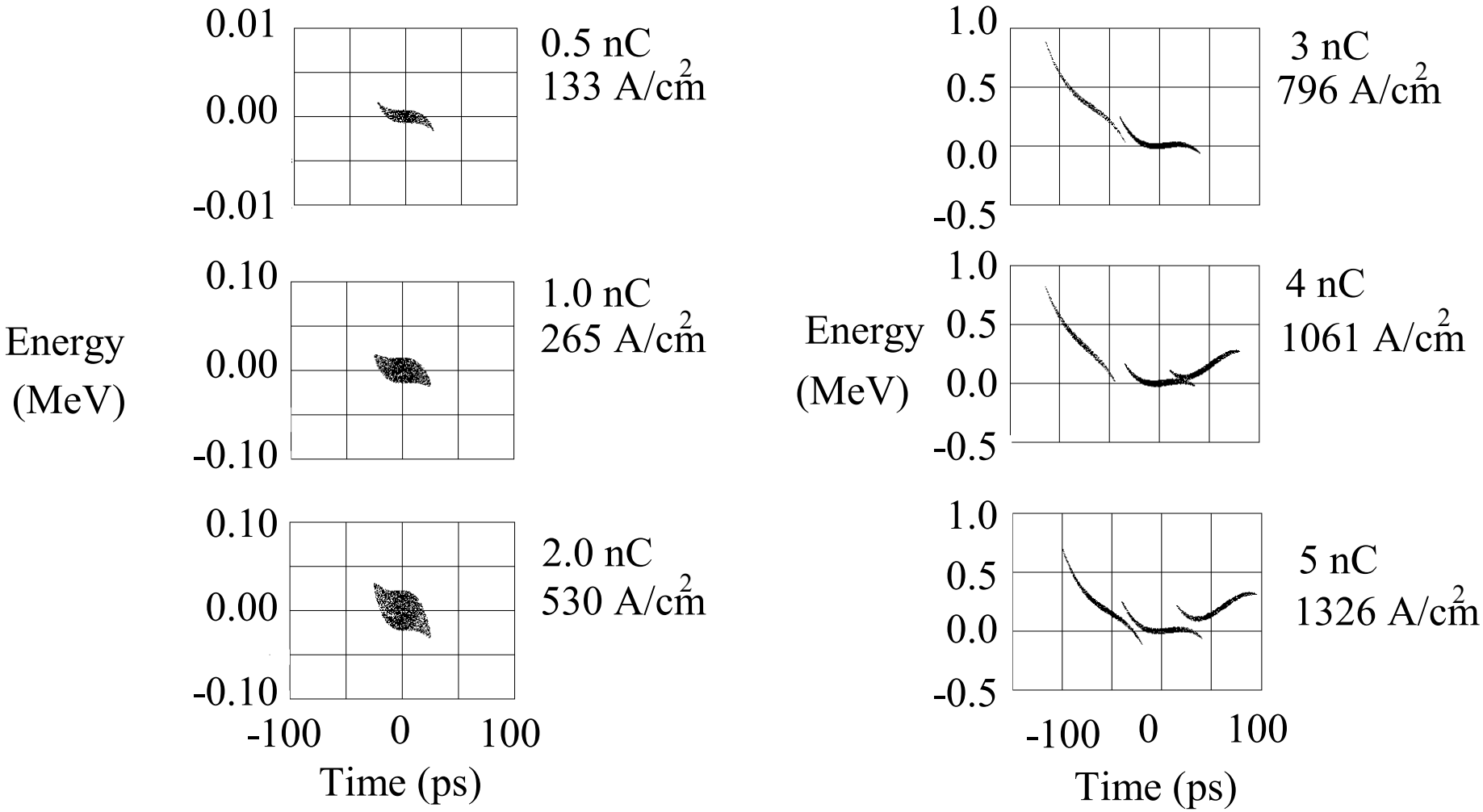

SIMPLE MODEL

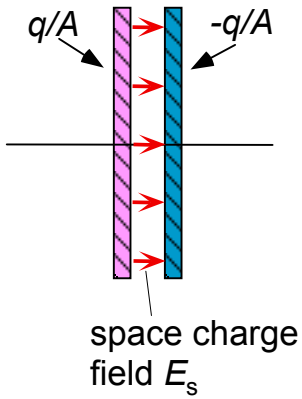

- Space charge field E_s increases as charge is photo-emitted from cathode surface

$$E_s = \frac{q}{A\varepsilon_o}$$

- Emission shuts off when it neutralizes the RF field E_o
- Maximum extractable charge is therefore

$$q_{mx} = \varepsilon_o E_o A = \frac{\pi \varepsilon_o E_o d^2}{4} = .2\ d^2 \frac{\text{nC}}{\text{mm}^2}$$

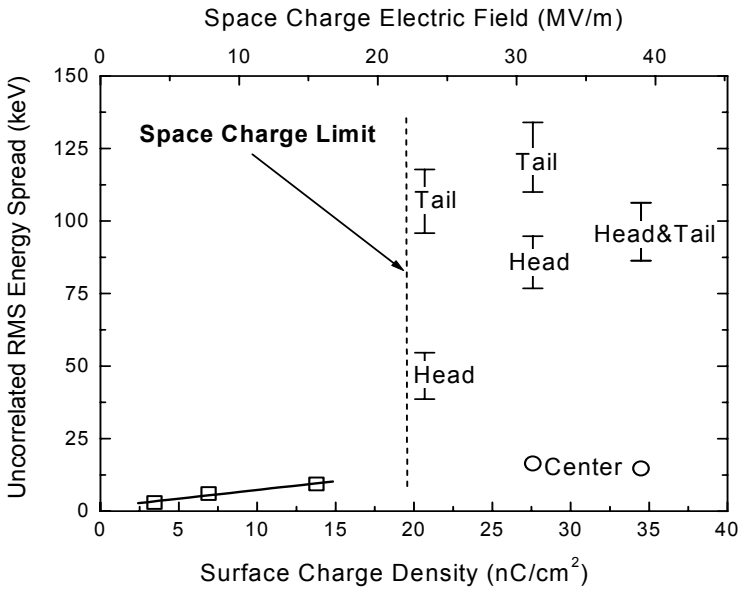

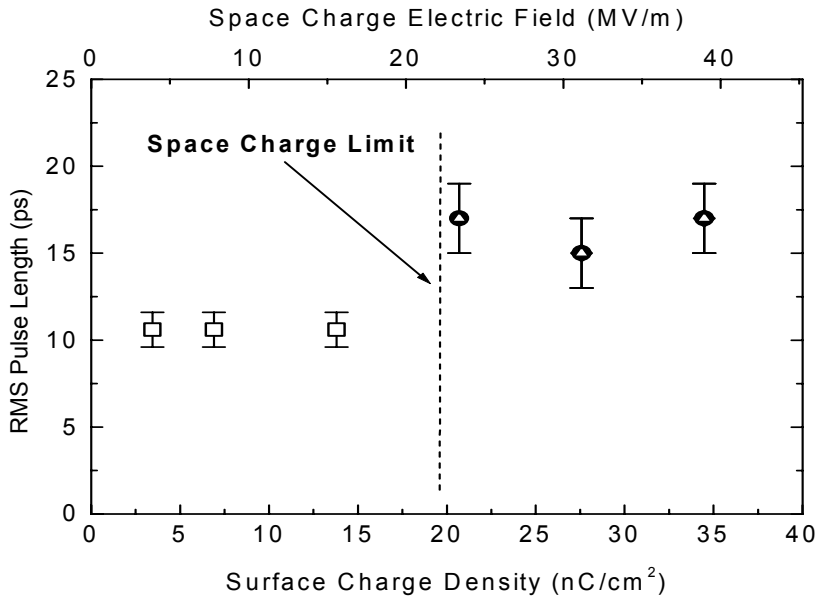

A 2 nC sphere of uniformly distributed charge introduces a ~3 MeV/m electric field near the cathode. The sphere approximately matches the dimensions of a micropulse and assumes the cathode is a perfect conductor.

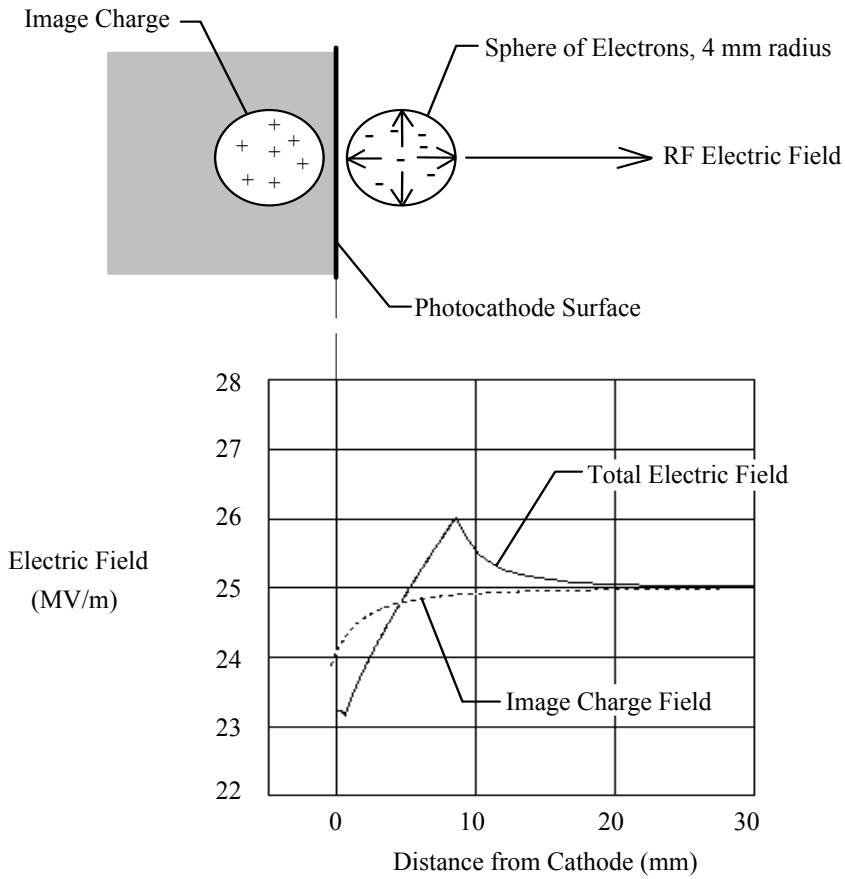

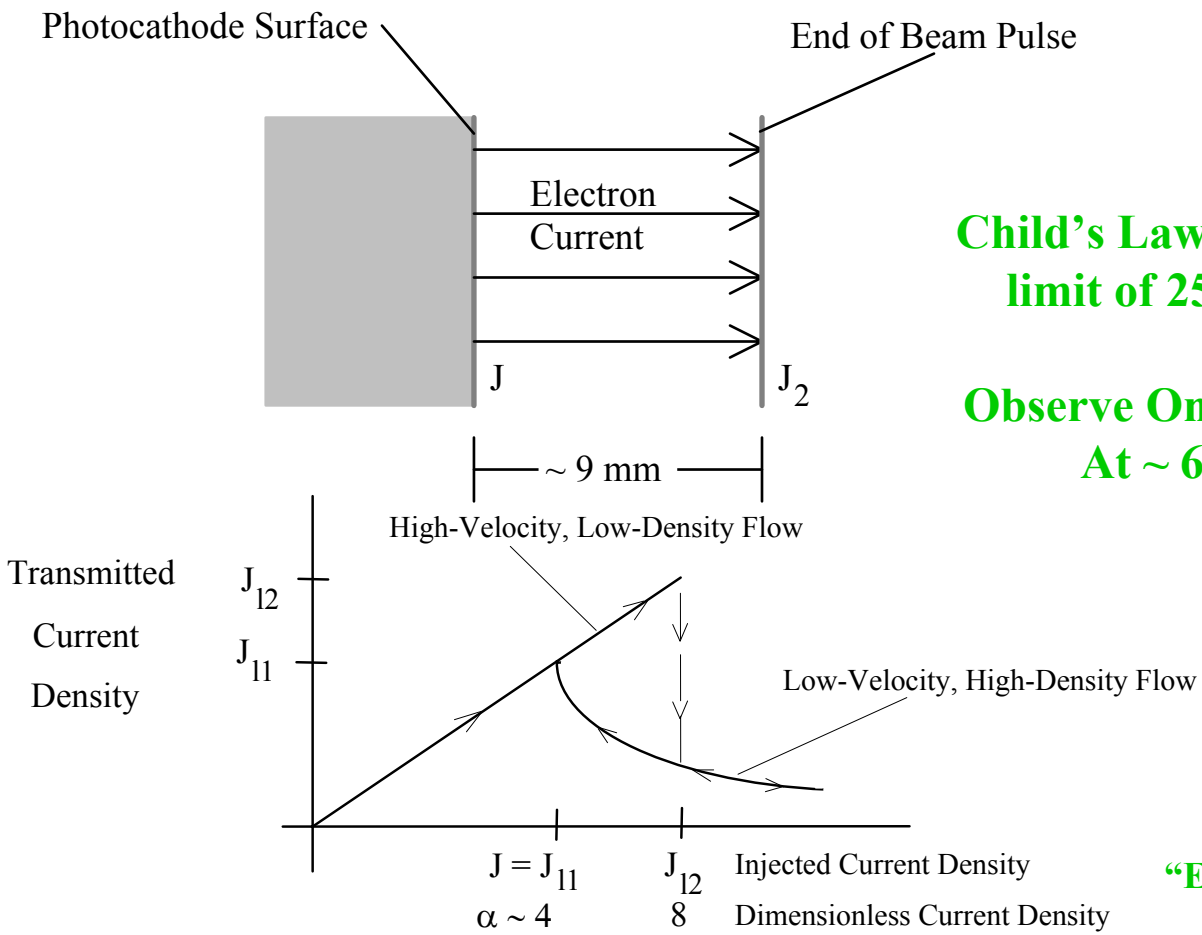

Child's Law gives the space charge limit of 250 A/cm^2 (rms) (α=1)

Observe Onset of Virtual Cathode At ~ 600 A/cm^2 (fwhm)

See Birdsall and Bridges, "Electron Dynamics of Diode Regions"

The transmitted current density as a function of the injected current density flowing between two infinite and parallel planes. Below J_{11}, the current flow is laminar and single-valued, while between J_{11} and J_{12} the flow can correspond to high-velocity, low-density flow (an extension of low current laminar flow) or to low-velocity, high-density flow. Above J_{12}, only low-velocity, high-density flow is present. The low-velocity, high-density flow is unstable, leading to formation of a virtual cathode midway between the planes.

Virtual Cathode Oscillation Frequency

The virtual cathode oscillation frequency as a function of distance from the photo-cathode. The βγ of the beam is computed assuming constant acceleration from the photo-cathode due to the 25 MV/m rf field.

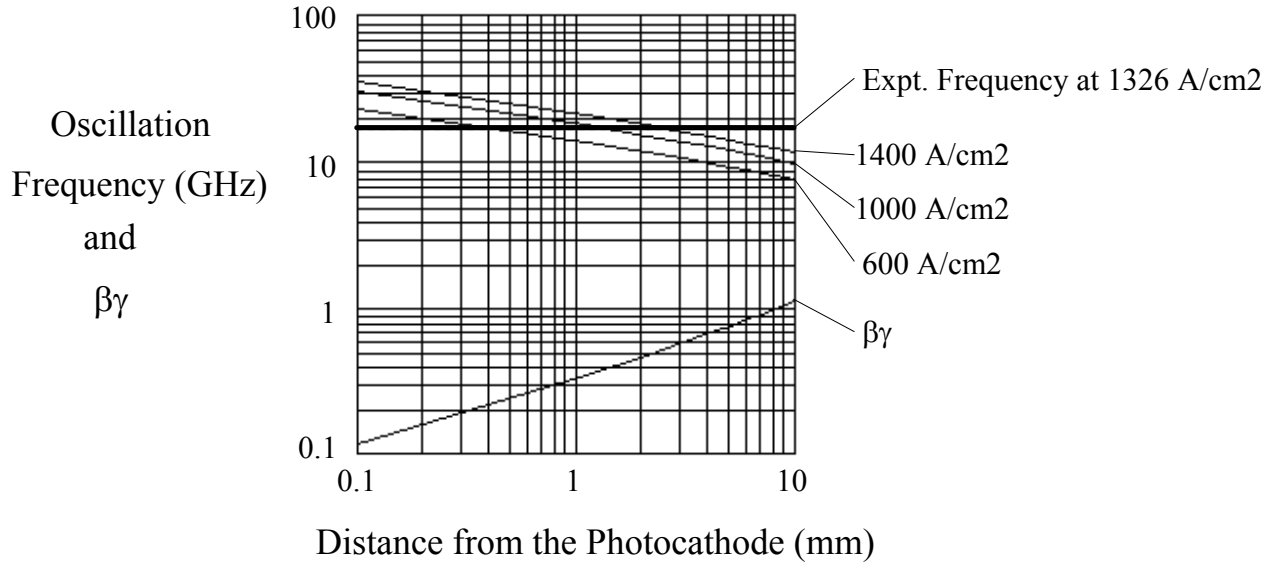

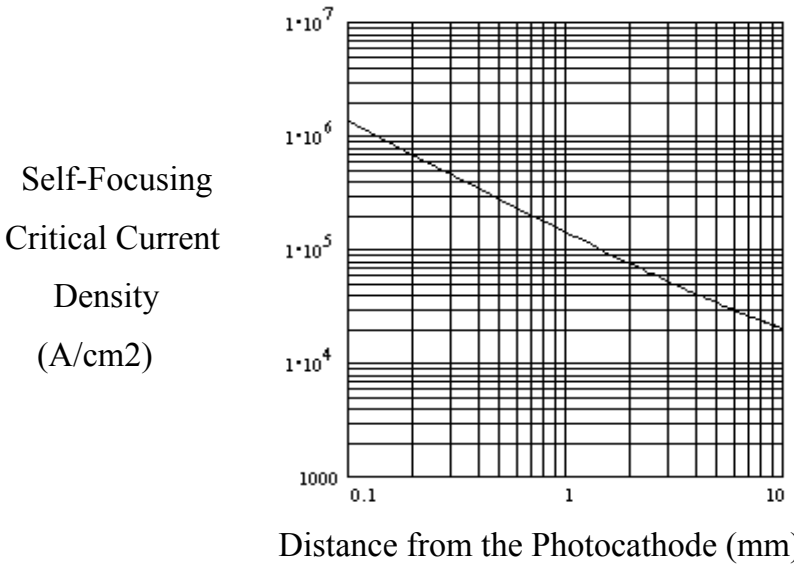

Current is far below self-focusing critical density.

Summary and Conclusions

- **Longitudinal Emittance Measured below the SCL**
- **Longitudinal Phase Space Distributions Reconstructed Using ART Tomography**
  - **For charges from 15 to 600 pC**
- **Tomography Essential for Separating Correlated and Uncorrelated Longitudinal Parameters**

- **Virtual Cathode Observed in RF Gun**
  - **Virtual cathode forms ~3-4 times Child's SCL**
  - **Results consistent with classical theory of Birdsall and Bridges**